remote sensing

MDPI

Article

Nighttime Tweek Characteristics in Mid–Low Latitudes: Insights from Long-Term VLF Observations in China

Qingshan Wang [1], Binbin Ni [1,2,*], Jingyuan Feng [1], Xudong Gu [1,2], Wei Xu [1,2], Shiwei Wang [1], Mengyao Hu [1], Wenchen Ma [1], Wen Cheng [1], Yufeng Wu [1] and Junjie Zhang [1]

[1] School of Earth and Space Science and Technology, Wuhan University, Wuhan 430072, China; wqs1118@whu.edu.cn (Q.W.); jingyuanf@whu.edu.cn (J.F.); guxudong@whu.edu.cn (X.G.); wei.xu@whu.edu.cn (W.X.); wangsw@whu.edu.cn (S.W.); humengyao@whu.edu.cn (M.H.); mawenchen@whu.edu.cn (W.M.); wencheng@whu.edu.cn (W.C.); yufengwu@whu.edu.cn (Y.W.); zhangjj0620@whu.edu.cn (J.Z.)

[2] Hubei Luojia Laboratory, Wuhan 430072, China

* Correspondence: bbni@whu.edu.cn

Abstract: An improved method for identifying nighttime tweek signals in WHU VLF measurements was developed by redesigning the extraction process and validated through comparison with World-Wide Lightning Location Network (WWLLN) data. Using the enhanced method, 1,728,032 tweek signals were identified from four years (2018–2021) of VLF data, forming the most comprehensive tweek dataset for the mid–low latitude region in China. Statistical analysis reveals distinct nighttime variations in tweek occurrence rates, which increase from 18:00 LT to 20:00 LT, remain high until 04:00 LT, and gradually decrease towards sunrise. Seasonal differences in propagation distance are evident, ranging from ~2000 km in summer to ~4000 km in winter, corresponding to the seasonal shift of lightning activity. The cutoff frequency showed apparent daily and seasonal fluctuations, and the trends of daily variation are opposite between winter and summer. The annual variation in cutoff frequency presents a pattern different from previous cognition, with a minimum of 1.62 kHz in summer and a maximum of 1.68 kHz in winter, influenced by the magnetic cyclotron frequency at ionospheric reflection points. These findings improve the understanding of nighttime tweek characteristics and ionospheric dynamics in East Asia, offering valuable insights for ionospheric research and VLF communication systems.

Keywords: very low frequency; tweek; automatic identification method; statistical analysis

check for updates

Academic Editor: Yunbin Yuan

Received: 17 December 2024
Revised: 21 January 2025
Accepted: 24 January 2025
Published: 27 January 2025

Citation: Wang, Q.; Ni, B.; Feng, J.; Gu, X.; Xu, W.; Wang, S.; Hu, M.; Ma, W.; Cheng, W.; Wu, Y.; et al. Nighttime Tweek Characteristics in Mid–Low Latitudes: Insights from Long-Term VLF Observations in China. *Remote Sens.* **2025**, *17*, 438. https://doi.org/10.3390/rs17030438

Copyright: © 2025 by the authors. Licensee MDPI, Basel, Switzerland. This article is an open access article distributed under the terms and conditions of the Creative Commons Attribution (CC BY) license (https://creativecommons.org/licenses/by/4.0/).

1. Introduction

Lightning discharges generate electromagnetic waves across a wide frequency spectrum, ranging from a few hertz to beyond the visible light range [1]. The majority of the energy radiated by lightning is concentrated in the extremely low frequency (ELF, 300 Hz–3 kHz) and very low frequency (VLF, 3 kHz–30 kHz) bands, with peak spectral density typically occurring below 15 kHz [2]. Among various signal sources in the VLF band, the electromagnetic pulses emitted by natural lightning discharges dominate [3]. Due to their low attenuation (2–3 dB per 1 Mm) through the Earth-Ionosphere Waveguide (EIWG), which is formed by the conductive ground and lower ionosphere [4], VLF emissions can propagate over distances of thousands to tens of thousands of kilometers, being reflected multiple times along the way. As a result, VLF wave detection systems are widely used to monitor lightning activity, providing valuable data for research on lightning phenomena and space environment remote sensing applications [5–12].

The VLF signals excited by lightning are called "atmospherics" or "sferics", and propagate in the EIWG with different wave modes. These wave mode have different electromagnetic field structures and, therefore, different group propagation speeds, so significant dispersion occurs at lower frequencies. When the wave frequency is lower than the cutoff frequency of the waveguide mode, the wave dissipates and rapidly attenuates. Among them, left-handed polarized waves are ultimately reflected in the lower ionosphere, forming "tweeks" due to significant dispersion within the EIWG in a short timescale [13–15]. Tweek may have multiple harmonic components, and high-order modes attenuate faster in the waveguide [16]. Right-handed polarized waves are transmitted to the outer ionosphere, propagating along the duct which is formed by field-aligned density inhomogeneities caused by plasma density enhancement or depletion [17–19], and can be thus observed by satellites and ground receiving stations in the other hemisphere, forming the so-called "whistlers" caused by the dispersion over a longer timescale [20,21]. In the spectrum, tweeks have a short vertical portion and a nearly horizontal portion lasting approximately 30 ms to 100 ms, while the cutoff frequency appears around 1.6–2.0 kHz [22,23]. In contrast, whistlers exhibit a slower decline in the spectrum, often lasting for several seconds.

Therefore, various VLF detection systems have been developed, including the Atmospheric Weather Electromagnetic System for Observation, Modeling, and Education receiver (AWESOME) [24] and the Antarctic-Arctic Radiation-belt Dynamic Deposition VLF Atmospheric Research Konsortia (AARDDVARK) [25]. Moreover, Wuhan University has developed another VLF detection system and deployed it in the middle- and low-latitude regions, the Tibetan Plateau, and the Great Wall station in Antarctica [9], constituting another reliable source of VLF measurements. Based on these observations, tweek-related studies continue to be conducted, leading to a deeper understanding of the characteristics and physical mechanisms.

Extensive efforts have been made to accurately and efficiently identify tweeks from observational data. In the early stage, tweek signals were manually processed and identified from VLF observation data, and then parameter extraction was carried out according to the dispersion characteristics. Then, the image processing method was developed to process the signal from the spectrum structure, and the maximum entropy spectrum estimation method was used to obtain the parameters automatically [26]. With the invention of Machine Learning and Artificial Neural Networks (ANNs), the method of using Deep Neural Networks for the target recognition of tweeks spectral signals has been widely applied [27–29]. Regarding tweeks recognition, the further extraction of propagation characteristic parameters can be carried out, often based on feature recognition in VLF spectrograms [30,31]. Based on the observational data, the evolution and distribution characteristics of tweeks are gradually revealed. The occurrence rate of tweeks has a significant diurnal variation because the typical attenuation factor of tweeks during the day can be as high as 70 dB/Mm, while the typical value at night is 3 dB/Mm [32,33]. Observing tweeks during the daytime is challenging unless a total solar eclipse occurs, while it can be observed in large quantities at night. Due to the small propagation attenuation factor at night, tweeks can propagate over long distances, with the vast majority reaching 4000–8000 km.

Tweek signals are a useful tool for ionospheric telemetry and are commonly employed in D-region ionospheric inversion [34–36]. Detecting the D-region ionosphere has long been challenging, as this altitude is inaccessible to both sounding balloons and satellites. Tweek signals provide an economical and effective method for determining parameters such as the height and electron density of the D-region ionosphere. The statistical analysis of tweek propagation characteristics plays a key role in enhancing our understanding of the temporal and spatial variations in the D-region. Such analyses offer valuable data to

improve ionospheric inversion techniques and refine existing models, contributing to more accurate ionospheric monitoring and advancing remote sensing applications. However, research on tweeks in the middle and low latitudes of China has been limited, and a systematic understanding of their characteristics is still lacking. This study addresses this gap by utilizing four years of VLF observation data from the Suizhou VLF station (31.57°N, 113.32°E) in Hubei, China. A total of 1,738,032 tweek signals were extracted from data collected between April 2018 and November 2021. We propose an effective automatic method for extracting tweek feature parameters, which forms the basis for constructing a comprehensive tweek database. A detailed statistical analysis explored the daily, monthly, and annual variations in the occurrence rate, propagation distance, and cutoff frequency of tweek signals. By integrating the WWLLN lightning location data, we analyze the underlying causes and mechanisms behind the observed statistical trends. The findings provide new insights into the evolution of tweek signals in middle and low latitudes, enhancing the understanding of D-region ionospheric behavior. This work contributes to the advancement of tweek research and promotes its application in D-region ionospheric remote sensing, with potential benefits for ionospheric monitoring and related technologies.

2. Database and Methodology

2.1. Instrument and Database

The VLF observation system designed by Wuhan University in Suizhou (31.57°N, 113.32°E) Hubei [37] was used to observe VLF signals continuously. The device consists of two magnetic loop antennas, a front-end amplifier, a GPS receiver, a digital acquisition board, and a host computer with a control program. The magnetic loop antenna, composed of coils with an air core, is arranged in the north-to-south and east-to-west directions, respectively, and the two are orthogonal to each other. The VLF signal is amplified by a front-end amplifier and sampled by the digital acquisition board using a 16-bit ADC at a sampling rate of 250 kHz. Using the GPS PPS signal, the digital acquisition board calibrated the local clock and the sampling time for the sampled data. The standardized digital signal is finally transmitted to the upper computer, processed, and stored in a "sampling 10 s—stopping 10 s, and repeating continuously" rule.

A YOLO object detection neural network model was used for automatic recognition and extraction [29], to obtain a tweek dataset that includes information such as the time of occurrence, original sampling data segments, duration, and cutoff frequency. Using 4-year VLF observations at Suizhou station, a preliminary database of tweek signals from April 2018 to November 2021 is constructed through the YOLO model described above. However, more accurate and verified data need to be obtained through further data processing, as described in Section 2.2.

The World-Wide Lightning Location Network (WWLLN, https://wwlln.net) is a lightning detection system that provides real-time lightning data by measuring the VLF signal radiated by lightning [38,39]. The system adopts multi-site positioning technology, which can obtain information including date and occurrence time (μs accurate level), latitude and longitude coordinates, and the number of stations recorded during the lightning event so that it can be used to obtain the distance and location of global lightning. The 4-year WWLLN data are used to verify our method and explain the underlying mechanisms.

2.2. Methodology

In order to obtain more accurate tweek parameters, we reprocess the original data corresponding to tweek events identified by the YOLO model. The sampling segment containing tweeks is obtained according to the information in the tweeks database, and 4096-point STFT (Short Time Fourier Transform) is performed on the sampling segment to get a

spectrum diagram in which it is easy to identify tweeks. Then, the characteristic parameters of tweeks are automatically identified and extracted from the spectrum. Considering that weak tweek signals are greatly affected by background noise interference, the incomplete spectral structure can lead to the failure of automatic propagation parameter extraction algorithms based on structural features. Therefore, we first normalize the spectrum to a maximum value of 0 dB and then set a decision threshold of −15 dB. Only tweek signals with intensities greater than this threshold were processed, forming the dataset used in this study.

We have redesigned the automatic extraction algorithm of tweeks to obtain more accurate information than previous studies [26,31,40]. Using the automatic extraction algorithm for tweeks, including trace recognition, outlier elimination, and separation of harmonic branches, independent branches of each order of harmonics can be obtained. The gradient method is used for trace recognition. Specifically, when a point in the spectrogram reaches its maximum value in the time or frequency axis, it is regarded as a candidate trace point. The clustering method is then utilized to process the candidate trace points and eliminate the outliers. Finally, branches of tweeks harmonics are identified based on the trend of the trace points. In Figure 1, as an example of parameter extraction, tweeks have a maximum of two harmonics, with blue points forming the branch of the first-order harmonic and red points forming the branch of the second-order harmonic. The propagation characteristic parameters can be extracted via the theoretical propagation equation of tweeks in EIWG [31],

$$f_n(t) = \frac{f_{cn}}{\sqrt{1 - \left(\frac{d}{c(t-t_0)}\right)^2}} \tag{1}$$

where n is the order of the waveguide mode, f_{cn} is the cutoff frequency of the nth order mode, d is the propagation distance, c is the speed of vacuum light, t is the time when the wave packet with a center frequency of f_n reaches the receiving station, and t_0 is the time when the related lightning occurs. By using Equation (1) and performing least squares fitting on the automatically extracted tweeks structure data points $(t, f_n(t))$, the nth-order mode tweek parameters, i.e., the cutoff frequency f_{cn}, propagation distance d, and lightning occurrence time t_0, can be obtained.

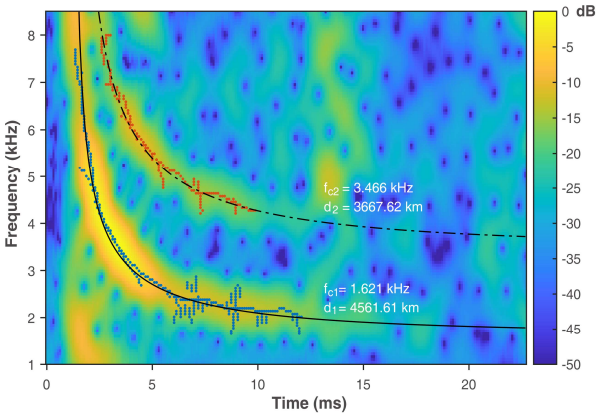


Figure 1. An example of tweek parameter extraction. The blue and red scatter points represent the two branches extracted by the automatic recognition algorithm, while the black solid and dashed lines indicate the fitting curves for the first-order and second-order harmonics, respectively. The corresponding frequency and propagation distance parameters are labeled in the figure.

In this example, characteristic parameters extraction is performed for the first-order and second-order harmonics. The cutoff frequency of the first-order harmonic is 1.621 kHz,

and the propagation distance is 4561 km, while the cutoff frequency of the second-order harmonic is 3.466 kHz, and the propagation distance is 3667 km. It should be noted that because the second harmonic is weak and the structure is incomplete, the propagation distance of the second harmonic is different from that of the first harmonic.

2.3. Validation

To ensure that the tweek signals originated from lightning events, we matched the tweek signals with lightning sources identified by the WWLLN system. The great circle distance between the lightning source and the Suizhou station was calculated using the latitude and longitude coordinates provided by WWLLN. Using the recorded lightning occurrence time and the formula $t_{arrival} = t_{WWLLN} + d_{WWLLN}/c$, where d_{WWLLN} is the great circle distance and c is the speed of light, we estimated the theoretical arrival time of the tweek signals at Suizhou station. A match was confirmed if the theoretical arrival time closely aligned with the actual arrival time of the tweek observed at Suizhou, within a time tolerance of ± 1 ms. This threshold was chosen to balance accuracy and reliability, as a larger tolerance could lead to incorrect matches, while a smaller tolerance might reduce the matching rate. To further ensure data quality, the propagation distance was limited to 6000 km, as excessive distances can degrade inversion results.

The extraction results are highly reliable, as the first-order harmonics, or the "basic tail" displayed in the spectrum, exhibit minimal attenuation and maintain a relatively complete structure. Consequently, the propagation distance of tweeks in this study specifically refers to the distance associated with first-order harmonics. Figure 2a,c,e,g present the correlation between propagation distances and WWLLN lightning distances for the equinoxes and solstices in 2020, specifically on 21 March, 22 June, 22 September, and 23 December. The corresponding Pearson correlation coefficients are R = 0.933, R = 0.942, R = 0.913, and R = 0.898, respectively, demonstrating a strong linear relationship between the two datasets. Additionally, Figure 2b,d,f,h show the relative distance ratio distributions between the propagation distance and WWLLN lightning distance on the same day. In most cases, the relative difference is less than 20%, which is a significant improvement over the 20–50% accuracy reported in previous studies [26,40]. These results indicate that the tweek signals extracted using the proposed method align well with lightning measurements, confirming the accuracy and reliability of the identification approach.

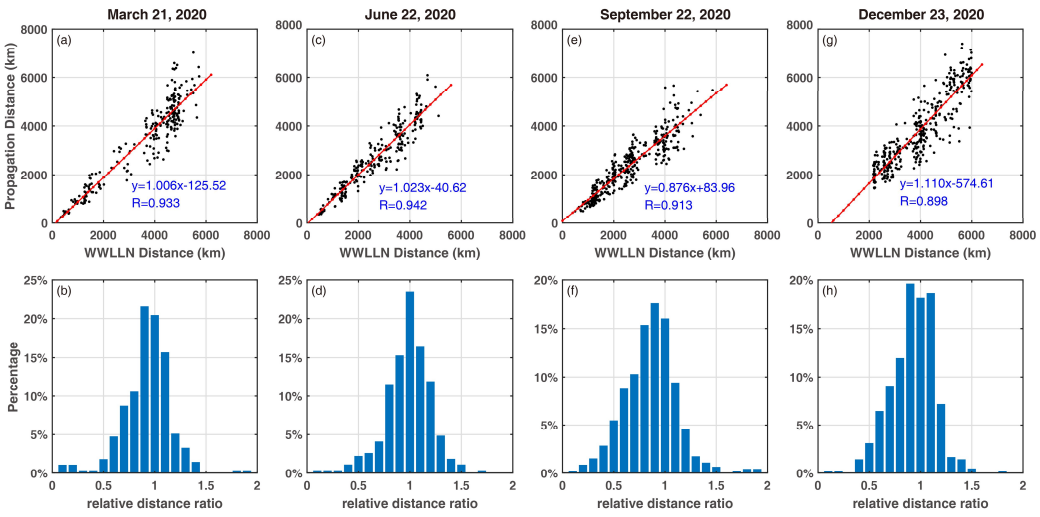


Figure 2. Panels (**a**,**c**,**e**,**g**) show the comparison between tweek propagation distance and WWLLN lightning distance on 21 March, 22 June, 22 September, and 23 December 2020, respectively. The red

dashed lines indicate the linear correlation, with correlation coefficients (R) of 0.933, 0.942, 0.913, and 0.898. Panels (**b**,**d**,**f**,**h**) present the distribution of the relative distance ratio α between tweek propagation distance and WWLLN lightning distance on the same days.

3. Statistical Results

3.1. Daily and Monthly Statistical Analysis

Based on the observation data collected at Suizhou station from April 2018 to November 2021, a total of 1,728,032 nighttime tweek signals were identified using the improved extraction method. To ensure data reliability, months with missing sampling data—November 2018 and March 2019 to May 2019—were excluded from the analysis. Considering that tweek signals occur predominantly at night [32,33], only data recorded between 18:00 LT and 06:00 LT the following day were used for the subsequent analysis, emphasizing the nighttime characteristics of tweek signals.

Figure 3 illustrates the hourly-averaged occurrence number of tweek signals during nighttime (18:00 LT to 06:00 LT) for each month from 2018 to 2021. The occurrence number shows a clear daily variation, which begins to increase from 18:00 LT, peaks around 20:00 LT to 22:00 LT, remains relatively stable until 04:00 LT, and then gradually decreases. This trend is consistent across the months but with varying magnitudes. The stabilization period from 20:00 LT to 04:00 LT corresponds to the extended nighttime propagation conditions that favor the transmission of tweek signals.

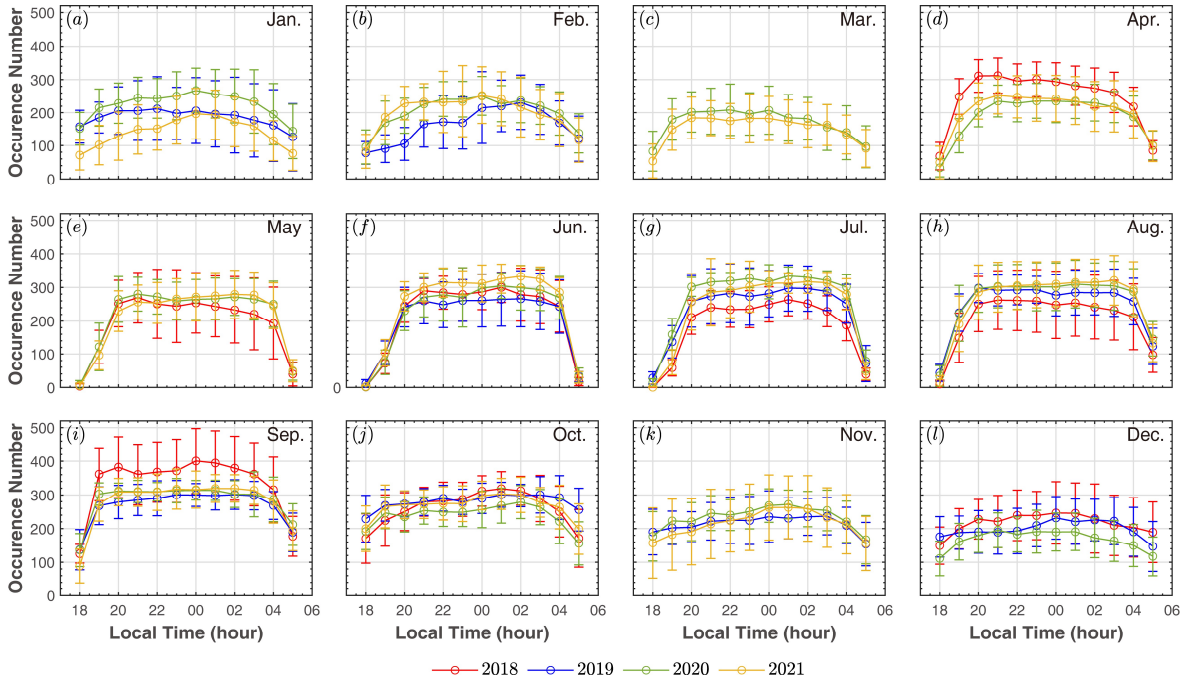


Figure 3. Hourly averaged occurrence numbers of tweeks during nighttime for each month from 2018 to 2021. Subfigures (**a**–**l**) correspond to January through December, with results for 2018, 2019, 2020, and 2021 shown by red, blue, green, and yellow lines, respectively. The error bars display the standard deviations of daily occurrences in the month.

Seasonal differences are notable. In winter and spring, tweek occurrences remain relatively high around 18:00 LT and 06:00 LT, likely due to earlier sunsets and later sunrises that extend nighttime propagation windows. In contrast, during summer (May to August), the occurrence number drops significantly around 18:00 LT and 06:00 LT, as the later sunset and earlier sunrise reduce nighttime propagation periods. The peak hourly occurrence number in summer reaches approximately 300, while in winter, it is around 200, reflecting

seasonal variability. These differences suggest that nighttime duration and associated signal propagation efficiency strongly influence the number of detectable tweek signals across seasons.

Figure 3b indicates a distinct difference in the occurrence pattern for February 2019 compared to other months. Specifically, peak activity was observed around 02:00 LT, and a stable period between 20:00 LT and 04:00 LT was not present. Additionally, during the period from sunset to 02:00 LT the following day, the occurrence in February 2019 was notably lower than in other years, suggesting reduced lightning activity. A similar observation can be made in the January data shown in Figure 3a, where interannual variations in occurrences are more pronounced compared to other months, reflecting differences in lightning activity levels in equatorial regions.

Figure 4 presents the hourly averaged propagation distance of tweeks during nighttime for each month from 2018 to 2021, with data first averaged hourly and then monthly. The results show an evident seasonal variation and distinct patterns in the winter to spring months compared to summer months. From October to April (winter to spring), the propagation distance exhibits a general decreasing trend over the nighttime hours. The maximum propagation distance, observed around 18:00 LT, ranges between 4000 and 5000 km, and it gradually decreases to a minimum value of approximately 3000 km near 06:00 LT, where it stabilizes. This trend highlights favorable nighttime propagation conditions during winter and spring.

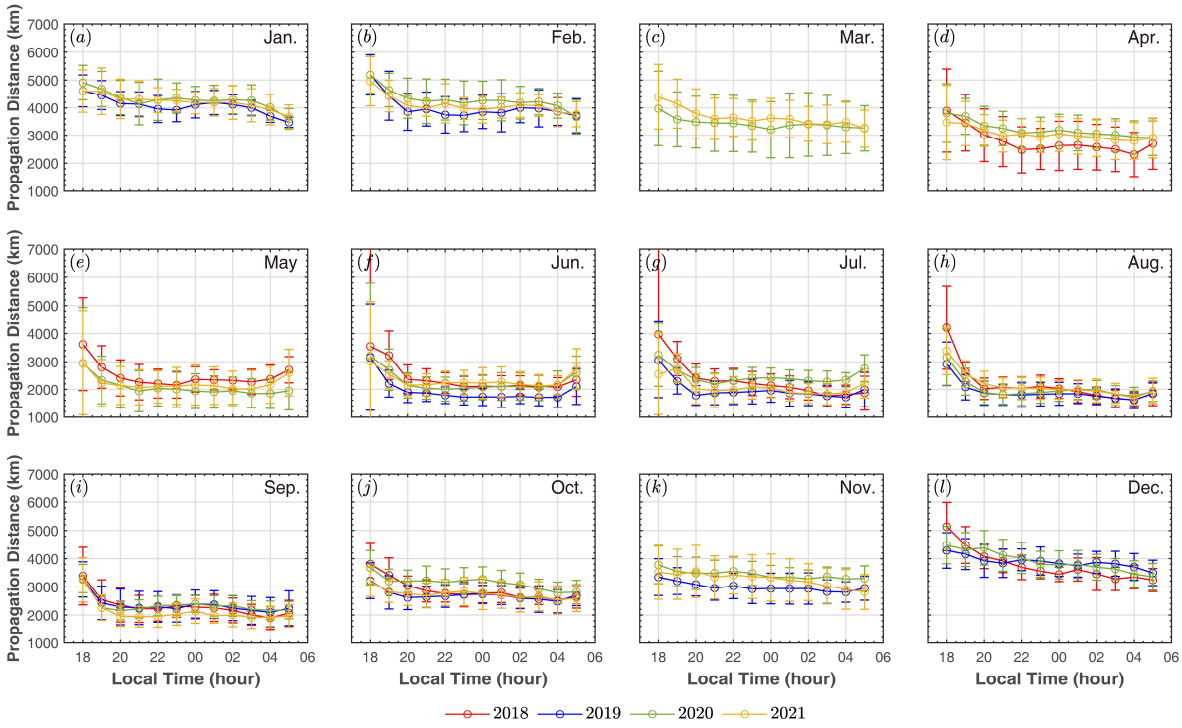


Figure 4. Hourly averaged propagation distance of tweeks during nighttime for each month from 2018 to 2021. Subfigures (**a**–**l**) correspond to January through December, with results for 2018, 2019, 2020, and 2021 shown in red, blue, green, and yellow, respectively. The error bars display the standard deviations of the daily average propagation distance for the month.

In contrast, during the summer months (May to August), the propagation distance displays a less pronounced bimodal structure, forming a distinct "W"-shaped pattern. Between 18:00 LT and 20:00 LT, the propagation distance drops sharply from around 3000–4000 km to approximately 2000 km. After this sharp decrease, the distance slightly increases to a local maximum around 01:00 LT, followed by a decline to a local minimum near 04:00 LT. Toward sunrise, the propagation distance increases again but remains lower than

the sunset values observed at 18:00 LT. Overall, this nighttime variation in summer reflects a more complex propagation environment, while the year-round pattern of propagation distance at nighttime shows a general downward trend as the night progresses.

Figure 5 shows the distribution of propagation distances of tweeks from 2018 to 2021, with propagation distances subdivided into 200 km intervals and grouped monthly. The statistical results reveal apparent seasonal variations in propagation distance distribution. From January to March, the distribution peaks around 4000 km, with an additional smaller peak at ~1000 km observed in February and March. This dual-peak pattern likely indicates multiple active lightning source regions at different distances during this period. From April to August, the peak propagation distance gradually decreases, reaching its minimum value of approximately 800 km in August. The peak distribution in April shows noticeable year-to-year variability, reflecting differences in the northward advance of the primary lightning source region.

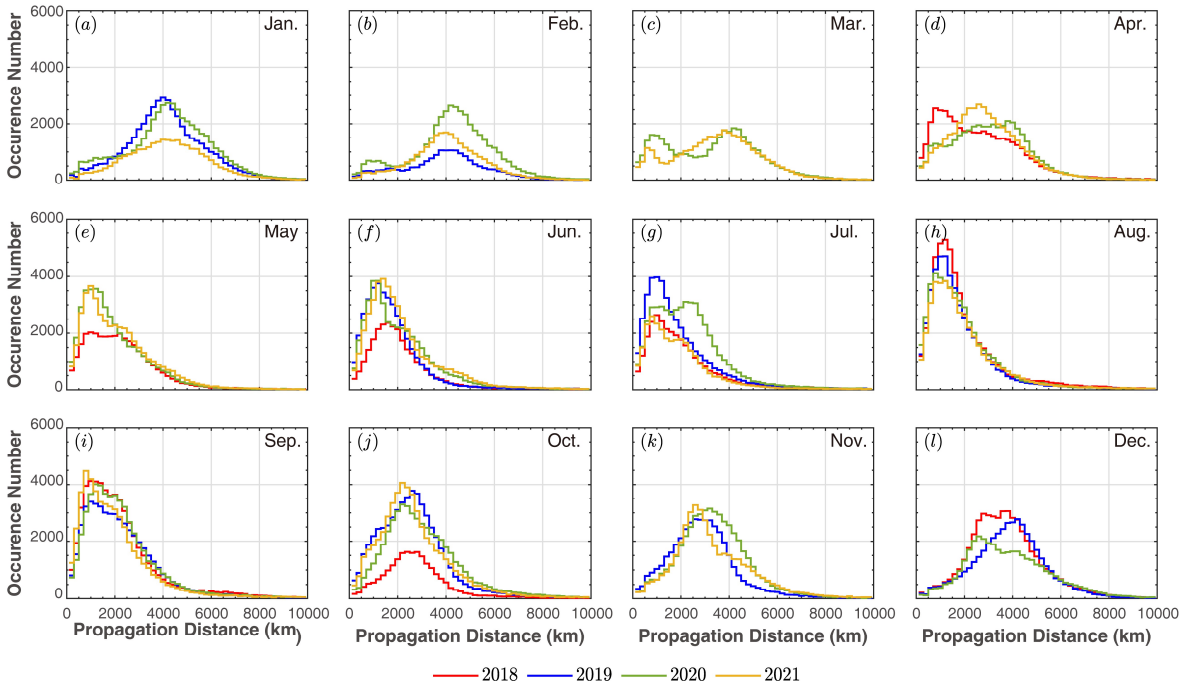


Figure 5. Distribution of tweek propagation distances for each month from 2018 to 2021. Subfigures (**a**–**l**) correspond to January through December, with results for 2018, 2019, 2020, and 2021 shown in red, blue, green, and yellow, respectively. The propagation distances are binned into 200 km intervals.

From September to December, the propagation distance gradually increases again, with the peak recovering to approximately 3000–4000 km by November and December. Similar to April, the peak distributions in December also show slight separation across different years, which reflects the southward retreat of the lighting source. These seasonal changes suggest shifts in the dominant lightning occurrence regions: during January to March, the likely source regions are southern China and Indonesia, while in July, the source regions appear to shift to southwest China and the Philippine Islands. The observed changes in the peak propagation distance effectively illustrate the seasonal movement of lightning activity, providing insights into the dynamic distribution of lightning sources across East Asia.

Figure 6 shows the daily variation of the monthly-averaged cutoff frequency of tweeks during nighttime from 2018 to 2021. In winter and spring, the cutoff frequency exhibits a gradual increase during the first half of the night, peaking at approximately 1.7 kHz around 00:00 LT, and then progressively decreases in the second half of the night. This trend

reflects changes in the lower ionospheric electron density, where recombination processes gradually reduce electron density as the night progresses. In contrast, during summer, the cutoff frequency follows the opposite pattern: it decreases from 18:00 LT to 22:00 LT, reaching a minimum of ~1.62 kHz, and then gradually increases until 06:00 LT, returning to a level of approximately 1.66 kHz.

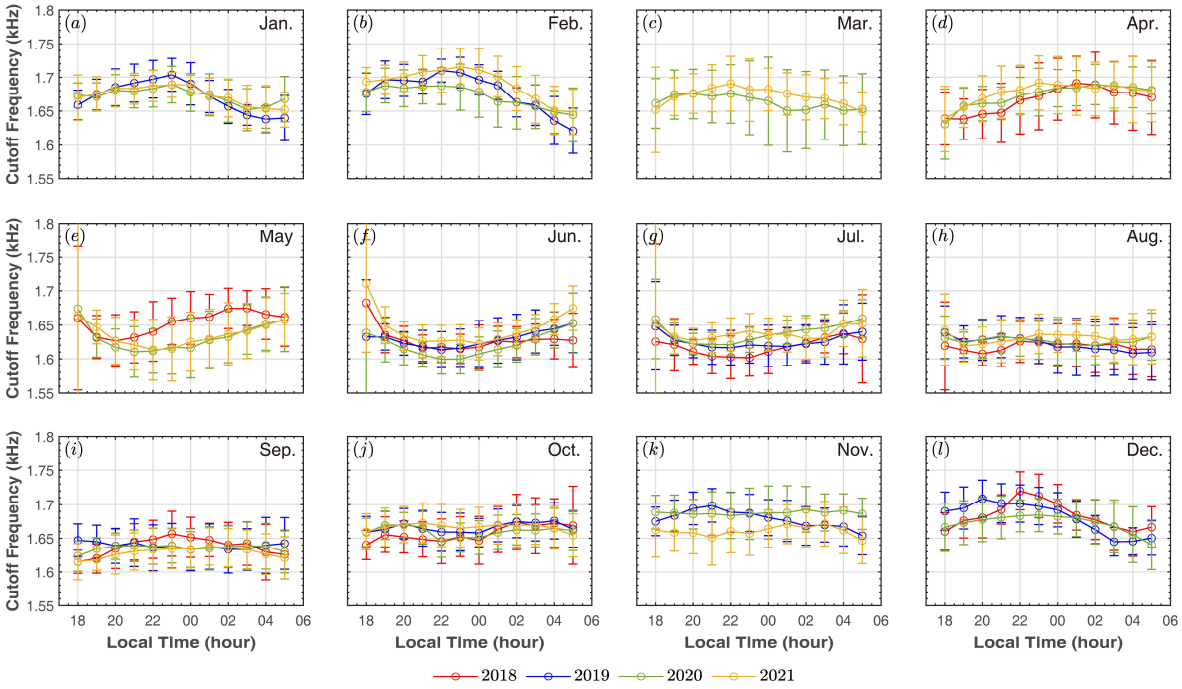


Figure 6. Hourly averaged cutoff frequency of tweeks during nighttime for each month from 2018 to 2021. Subfigures (**a**–**l**) correspond to January through December, with results for 2018, 2019, 2020, and 2021 shown in red, blue, green, and yellow, respectively. The error bars display the standard deviations of the daily average cutoff frequency for the month.

The transition between these two seasonal patterns occurs rapidly during the spring-to-summer transition (April to May). Notably, in May 2018, the transition was slower than in other years, with the cutoff frequency exhibiting an intermediate state between the two patterns. During the summer-to-winter transition (August to November), the pattern transformation is much slower, spanning several months. This difference suggests an asymmetry in the ionospheric seasonal response, where changes from summer to winter occur more gradually compared to the rapid onset of summer conditions. Overall, the monthly-averaged cutoff frequency ranges between 1.6 kHz and 1.7 kHz throughout the year.

A key observation is that the cutoff frequency of tweeks in East Asia does not display a monotonic downward trend throughout the night as in other regions, as reported in previous studies [20,34–36]. Instead, the behavior of the cutoff frequency reflects season-dependent ionospheric variations. In general, the cutoff frequency in the second half of the night is lower than in the first half (except for April), which aligns with the expected decrease in electron density due to recombination processes. The seasonal differences in the cutoff frequency patterns suggest complex dynamics in the D-region ionosphere, particularly its electron density variation in summer and winter, although the exact physical mechanisms remain unclear due to the ionosphere's inherent complexity.

3.2. Annual Statistical Analysis

A total of 1,738,032 tweek signals observed at the Suizhou station from April 2018 to November 2021 were statistically analyzed. Figure 7 presents the annual variation of monthly-averaged tweek parameters observed at the Suizhou station from April 2018 to November 2021. Figure 7a displays the occurrence number of tweeks, Figure 7b shows the propagation distance, and Figure 7c depicts the cutoff frequency. Significant seasonal variations are observed in all three parameters, reflecting the influence of seasonal lightning activity and ionospheric conditions.

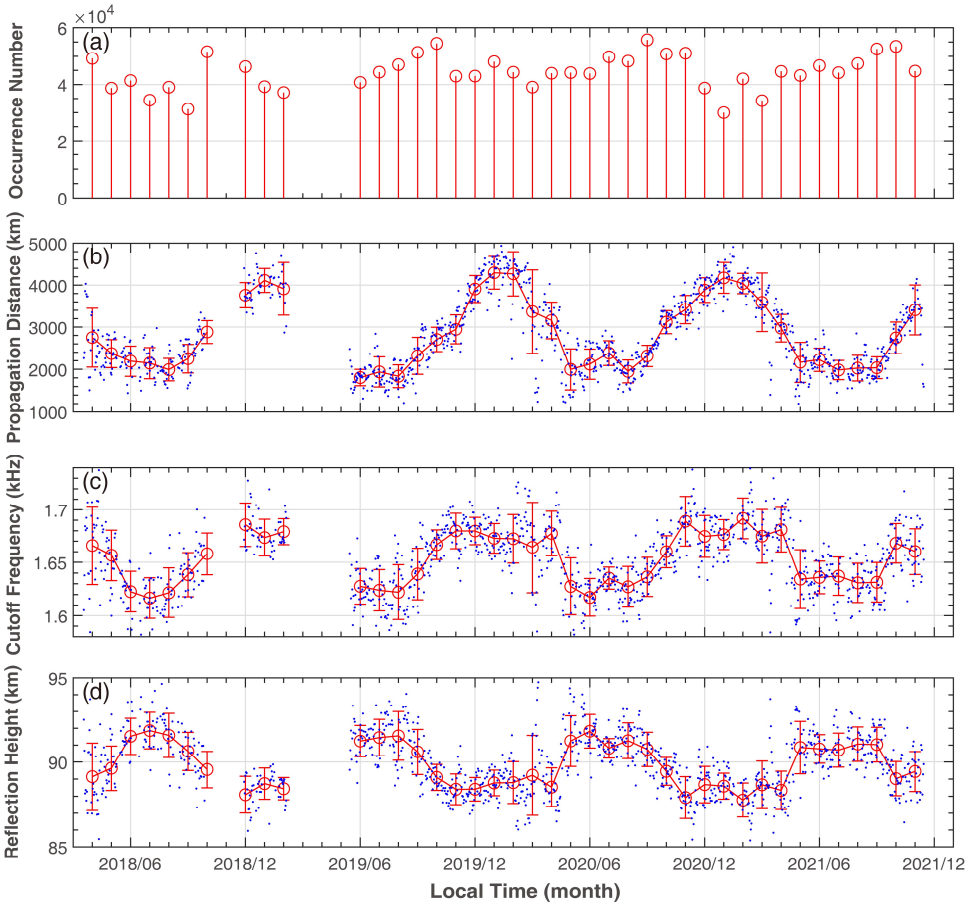


Figure 7. Monthly averaged characteristics of tweeks from 2018 to 2021. (**a**) Total occurrence numbers per month. (**b**) Propagation distance, with the red line representing the monthly average and blue scatter points showing daily values. (**c**) Cutoff frequency, with the red line indicating the monthly average and blue scatter points representing daily values. (**d**) Reflection height, with the red line indicating the monthly average and blue scatter points representing daily values. The error bars in (**b**–**d**) display the standard deviations.

In Figure 7a, the occurrence number of tweeks demonstrates a clear seasonal pattern. The number of occurrences is highest during summer and autumn (August and September), with monthly totals reaching nearly 60,000 cases, while the occurrence number is significantly lower in winter and spring (February and March), dropping to 20,000–30,000 cases. This seasonal variation aligns well with the East Asian monsoon region's lightning activity, where thunderstorms are more frequent during summer and early autumn due to enhanced convective activity. Conversely, in winter and early spring, reduced lightning occurrence results in a lower number of detected tweek signals.

Figure 7b shows the annual variation of propagation distance, which exhibits an apparent periodicity with a cycle of about one year. During winter (November to April),

the propagation distance reaches its maximum, with values extending up to 4200 km in January. This is attributed to the fact that during winter, lightning activity primarily occurs in the equatorial region, far from the Suizhou station, allowing tweek signals to propagate over longer distances. In contrast, during summer (May to August), the propagation distance is much shorter, reaching a minimum of approximately 1900 km, as the primary lightning activity shifts to the closer regions of South China and the Western Pacific.

Figure 7c illustrates the annual variation of the cutoff frequency, which also shows a distinct seasonal periodicity. The cutoff frequency is lower during summer, with a minimum value of approximately 1.62 kHz observed from June to August. In winter, the cutoff frequency is higher, reaching about 1.68 kHz, and this level is maintained from November to April. This variation is consistent with findings in Japan and Vietnam [36], where lower cutoff frequencies were reported in summer.

Figure 7d illustrates the annual variation of the reflection heights, showing that the reflection heights of tweek signals exhibit seasonal fluctuations. Higher reflection heights are observed during the summer months, while lower reflection heights are seen in the winter months. From November to April, the reflection height remains relatively low, around 88 km. Starting in May, the reflection height increases, reaching 91–92 km, and remains at this level until September, after which it gradually decreases. On average, the reflection height of tweeks observed in Suizhou is approximately 90 km, consistent with observations in Japan [32,36], but higher than those reported in Vietnam [23,36] and Fiji [20].

The distinct periodic variations of propagation distance and cutoff frequency highlight the seasonal movement of lightning activity and its relationship with ionospheric conditions. During winter, lightning is concentrated near the equatorial region, leading to longer propagation distances, while in summer, lightning activity in closer regions reduces the propagation distance. The seasonal variation of the cutoff frequency in East Asia, differing from previous studies in India [35] where higher summer values were observed, may be influenced by the latitude of the reflection point of tweek signals propagating in the Earth-Ionosphere Waveguide (EIWG). These observations, supported by large-scale statistical analysis, provide valuable insights into the interaction between lightning activity, ionospheric electron density, and seasonal propagation conditions. Based on the long-term and large-scale observation and combined with the WWLLN lightning location dataset, we propose another possible explanation for the abnormal seasonal differences in cutoff frequency in East Asia that the latitudes of the reflection point of tweeks propagating in the EIWG waveguide may play a significant role in the seasonal variation of the cutoff frequency, which will be discussed in Section 4.

4. Discussion

Tweek is a left-hand polarized wave that propagates quasi-longitudinally, and according to the Appleton-Hartree formula [41,42], ignoring particle collisions, the refractive index n satisfies,

$$n^2 = 1 - \frac{X}{1+Y},\ X = \frac{f_p^2}{f^2},\ Y = \frac{f_H}{f} \tag{2}$$

where $f_p = \frac{1}{2\pi}\sqrt{\frac{n_e e^2}{m_e \varepsilon_0}}$ is the plasma frequency and $f_H = \frac{eB}{2\pi m_e}$ is the magnetic cyclotron frequency, with the amount of electronic charge e, the mass of electrons m_e, the magnetic field intensity B, and the vacuum dielectric constant ε_0. The VLF wave is fully reflected

in the D-region ionosphere at frequency f_c, where the refraction index $n = 0$, and the corresponding electron density can be derived from Equation (2),

$$n_e = \frac{4\pi^2 m_e \varepsilon_0}{e^2} f_c(f_c + f_H) \tag{3}$$

According to the magnetic field intensity provided by the International Geomagnetic Reference Model (IGRF), the f_H in the middle and low latitude D-region ionosphere is estimated to be between 1.1 MHz and 1.3 MHz. Due to $f_c \ll f_H$, there is an approximate expression of Equation (3) about f_c as follows,

$$f_c \approx \frac{e^2}{4\pi^2 m_e \varepsilon_0} \cdot \frac{n_e}{f_H} \tag{4}$$

In terms of Equation (4), the cutoff frequency f_c of tweek is inversely proportional to the electron cyclotron frequency, which depends on the local magnetic field strength. At 90 km altitude and 120°E longitude, the cutoff frequencies corresponding to different typical D-region ionospheric electron densities vary with latitude, as shown in Figure 8. There is a significant difference in cutoff frequency at various latitudes. Due to the stronger magnetic field at high latitudes, the cyclotron frequency of electrons is relatively high, so the tweeks reflected through this area have a lower cutoff frequency. The latitude of the reflection point is extended from the equator to 30°N, and the cutoff frequency can be reduced by ~0.5 kHz. In addition, a meaningful increase in electron density leads to an increase in the plasma frequency, which can increase the cutoff frequency by about ~0.8 kHz as the electron density increases from 20 to 30 el./cm^3. Generally, the D-region ionosphere has a reflection height upper limit of 100 km, corresponding to a first-order cutoff frequency of 1.5 kHz, which is the lowest frequency that can be reflected by the D-region. This frequency is represented by the black dashed line in the graph. The results presented in Figure 8 show that the reflection frequency is influenced by both the background electron density and the magnetic field. Notably, variations in the magnetic field, driven by differences in latitude, play a key role in causing variations in the cutoff frequency at different latitudes.

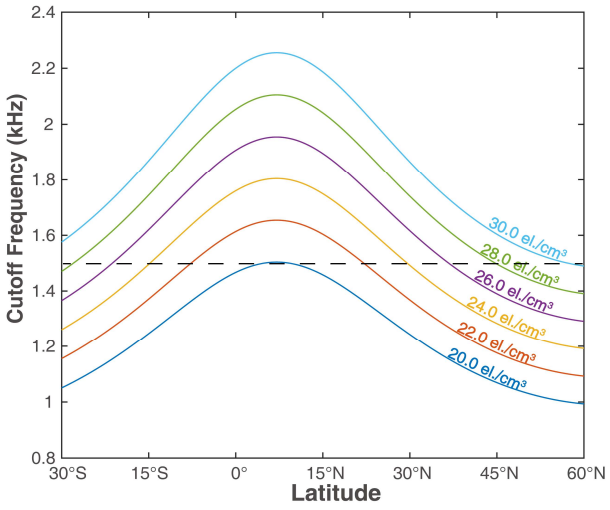


Figure 8. The variation of cutoff frequency with different latitudes and electron densities. Investigate under the condition of longitude at 120°E and altitude at 90 km, with latitude range of 30°S to 60°N and electron density range of 20 el./cm^3 to 30 el./cm^3. The first-order cutoff frequency corresponding to the D-region reflection height upper limit of 100 km is 1.5 kHz, which is represented by the black dashed line.

Figure 9 shows the distribution of WWLLN lightning matched with tweeks in different typical months of 2020, only counting lightning events within 6000 km from the Suizhou station. The red asterisk shows the observation station, the blue point represents the source locations of WWLLN lightning, and the green point represents the reflection point, roughly the midpoint of the tweek propagation path. It is evident that the average latitude of tweek reflection points is mainly distributed between 20°N and 30°N in June and extends to the lower latitude between 10°N and 20°N in December.

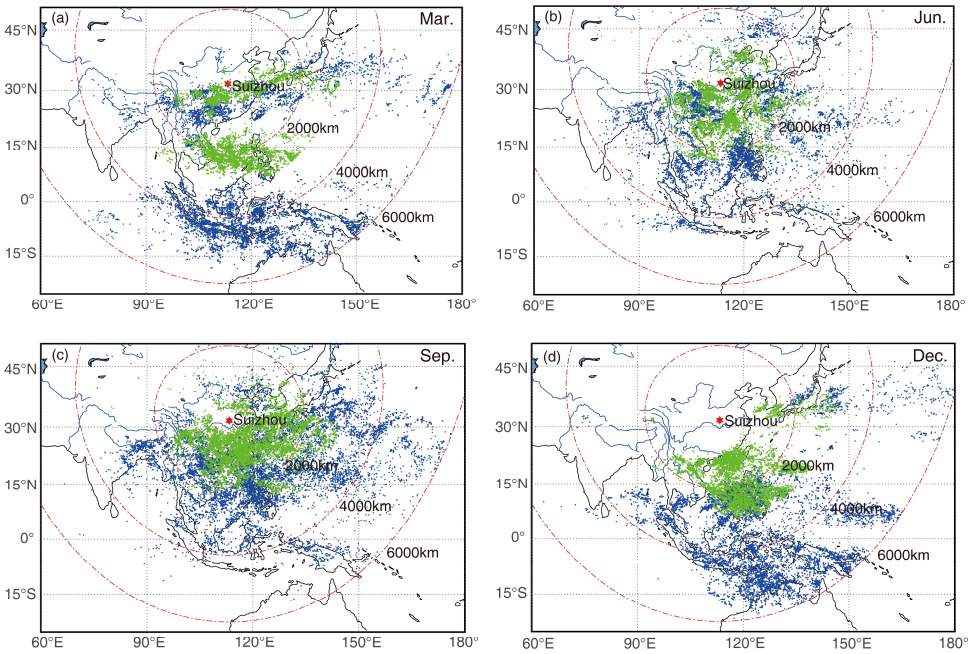


Figure 9. Distribution of matched WWLLN lightning in different seasons in 2020. Subfigures (**a**–**d**) respectively show lightning distribution around China in March, June, September, and December in 2020. The blue scatter corresponds to the lightning location, while the green scatter marks the midpoint of the propagation path.

According to the seasonal migration pattern of the causative lightning occurrence area shown in Figure 9, the distribution of propagation distance shown in Figure 5 can also be explained further. In January, causative lightning mainly occurs in Indonesia and its surrounding areas, corresponding to a peak distance distribution of ~4000 km, consistent with the distance to Suizhou Station. In February, a small amount of lightning occurred in southwestern China and the Western Pacific, while a large amount occurred in Indonesia areas, resulting in two peaks distributed at ~1000 km and ~4000 km, with the former being smaller. After entering March, lightning strikes significantly increased in the southern foothills of the Himalayas, southern China, and the western Pacific region. At the same time, the number of lightning strikes in Indonesia decreased slightly, but there were still many lightning strikes. Therefore, a clear bimodal structure was generated in the distribution, and the two peaks were roughly equal. After April and May, the number of lightning strikes in Indonesia decreased, and lightning strikes in the Indochinese Peninsula, South China and North China, South China Sea, and Western Pacific region significantly increased, resulting in peak distance distribution gradually appearing within the range of 1000–2000 km. The lightning mainly occurred in areas moving northward, which continued until August and then moved back southward. It retreated to the Philippines and the Western Pacific region in October, corresponding to a peak distance distribution at ~2200 km. In November and December, it retreated to Indonesia areas, corresponding to a peak distance distribution at 3400–4000 km.

5. Conclusions

In this study, a new automatic method for extracting tweek parameters was developed and validated by comparing it with WWLLN lightning discharge data. Based on four years of VLF observation data (April 2018 to November 2021) from the Suizhou station, a comprehensive nighttime tweek dataset for the mid-low latitude region was created, offering unprecedented insights into tweek signal characteristics. The analysis revealed significant findings on the diurnal, seasonal, and annual variations in tweek occurrence rates, propagation distances, and cutoff frequencies. Of particular note, the annual variation of the cutoff frequency exhibits a distinctive seasonal pattern, with lower values in summer and higher values in winter, contrasting with previously reported trends. This behavior is effectively explained by the influence of the magnetic cyclotron frequency at ionospheric reflection points, which is closely related to the seasonal north-south migration of lightning activity. The main conclusions of this study are as follows:

(1) Tweek occurrence rates exhibit a strong diurnal pattern, gradually increasing from 18:00 LT to 20:00 LT, maintaining a high level until 04:00 LT, and then decreasing before sunrise. Seasonal variations are pronounced at 18:00 LT and 06:00 LT: significant tweek activity occurs in winter, while signals are almost absent in summer due to the later sunset and earlier sunrise during summer months.

(2) The propagation distance shows a decreasing trend at nighttime with seasonal variability. In winter, distances decrease gradually from ~5000 km at sunset to ~3000 km near sunrise. In summer, the decrease is more abrupt, ranging from ~4000 km to a minimum of ~2000 km, followed by a slight increase around sunrise. In addition, the monthly averaged propagation distance varies with the season, descending from ~4000 km in winter to ~2000 km in summer. The seasonal migration of lightning sources, shifting northward in summer and southward in winter, explains the observed variations in propagation distance.

(3) The cutoff frequency shows distinct daily and seasonal differences. In summer, it decreases before 22:00 LT, then increases until sunrise, whereas in winter, it increases after sunset, peaks around 23:00 LT, and decreases towards morning. On an annual scale, the cutoff frequency is lower in summer (~1.62 kHz) and higher in winter (~1.68 kHz). This pattern reveals the latitude of causative lightning, more precisely, the corresponding magnetic cyclotron frequency of the reflection point along the propagation path, plays a significant role in the annual variation of cutoff frequency.

These findings enhance our understanding of tweek signal characteristics and their relationship with D-region ionospheric electron density variations in middle and low latitudes. The results provide valuable insights for ionospheric remote sensing and seasonal lightning monitoring. Future research can extend this methodology to different latitudinal regions, improve extraction accuracy, and explore the impacts of solar activity and geomagnetic disturbances on tweek parameters, further strengthening the application of VLF signals as a robust tool for ionospheric research.

Author Contributions: Data curation, X.G., S.W. and Q.W.; methodology, X.G., Q.W., W.X., W.M., J.F. and S.W.; validation, X.G., Q.W., W.X., M.H. and W.M.; investigation, W.X., X.G., Q.W., Y.W., J.Z., W.C. and J.F.; writing—original draft preparation, Q.W., X.G. and W.X.; writing—review and editing, X.G., W.X., Q.W., W.C, J.F. and B.N.; project administration, X.G., W.X., S.W. and B.N.; funding acquisition, X.G., B.N. and W.X. All authors have read and agreed to the published version of the manuscript.

Funding: This work was supported by the National Natural Science Foundation of China (Grant Nos. 42025404, 42188101, 42274205, and 42130210), the National Key R&D Program of China (Grant No. 2022YFF0503700), the open fund of Hubei Luojia Laboratory (Grant No. 220100051), and the Tencent Xplorer prize. The authors acknowledge the 985-funded project of Wuhan University.

Data Availability Statement: The processed VLF data used to generate the plots reported in this paper can be obtained from https://zenodo.org/records/14740965. More VLF data can be obtained after a request to Xudong Gu (guxudong@whu.edu.cn).

Acknowledgments: We are grateful to the Editor and anonymous reviewers for their assistance in evaluating this paper.

Conflicts of Interest: The authors declare no conflict of interest.

References

1. Prasad, R.; Singh, R.N. Various features of VLF waves generated by lightning discharge. *Il Nuovo C. C* **1982**, *5*, 462–476. [CrossRef]
2. Volland, H.; Schmolders, M.; Prölss, G.W.; Schäfer, J. VLF propagation parameters derived from sferics observations at high southern latitudes. *J. Atmos. Terr. Phys.* **1987**, *49*, 33–41. [CrossRef]
3. Kishore, A.; Deo, A.; Kumar, S. Upper atmospheric remote sensing using ELF–VLF lightning generated tweek and whistler sferics. *South Pac. J. Nat. Appl. Sci.* **2016**, *34*, 12–20. [CrossRef]
4. Yamashita, M. Propagation of tweek atmospherics. *J. Atmos. Terr. Phys.* **1978**, *40*, 151–156. [CrossRef]
5. Thome, G.D.; Wagner, L.S. Electron density enhancements in the E and F regions of the ionosphere during solar flares. *J. Geophys. Res.* **1971**, *76*, 6883–6895. [CrossRef]
6. Rodger, C.J.; Clilverd, M.A.; Thomson, N.R.; Gamble, R.J.; Seppälä, A.; Turunen, E.; Meredith, N.P.; Parrot, M.; Sauvaud, J.; Berthelier, J. Radiation belt electron precipitation into the atmosphere: Recovery from a geomagnetic storm. *J. Geophys. Res. Space Phys.* **2007**, *112*, A11307. [CrossRef]
7. Kumar, S.; Kumar, A.; Maurya, A.K.; Singh, R. Changes in the D region associated with three recent solar eclipses in the South Pacific region. *J. Geophys. Res. Space Phys.* **2016**, *121*, 5930–5943. [CrossRef]
8. Singh, R.; Veenadhari, B.; Maurya, A.K.; Cohen, M.B.; Kumar, S.; Selvakumaran, R.; Pant, P.; Singh, A.K.; Inan, U.S. D-region ionosphere response to the total solar eclipse of July 22 2009 deduced from ELF-VLF tweek observations in the Indian sector. *J. Geophys. Res. Space Phys.* **2011**, *116*, A10301. [CrossRef]
9. Gu, X.; Wang, Q.; Ni, B.; Xu, W.; Wang, S.; Yi, J.; Hu, Z.; Li, B.; He, F.; Chen, X.; et al. First results of the wave measurements by the WHU VLF wave detection system at the Chinese Great Wall station in Antarctica. *J. Geophys. Res. Space Phys.* **2022**, *127*, e2022JA030784. [CrossRef]
10. Gu, X.; Yi, J.; Wang, S.; Hu, Z.; Xu, W.; Ni, B.; Li, B.; He, F.; Chen, X.; Hu, H. Comparison of VLF signal responses to solar flares along daytime and nighttime propagation paths. *Remote Sens.* **2023**, *15*, 1018. [CrossRef]
11. Xu, W.; Marshall, R.A.; Kero, A.; Turunen, E.; Drob, D.; Sojka, J.; Rice, D. VLF measurements and modeling of the D-region response to the 2017 total solar eclipse. *IEEE Trans. Geosci. Remote Sens.* **2019**, *57*, 7613–7622. [CrossRef]
12. Xu, W.; Gu, X.; Ni, B.; Wang, S.; Yang, Z.; Cheng, W.; Hu, Z.; He, F.; Li, B.; Chen, X.; et al. Measurements and Modeling of the Responses of VLF Transmitter Signals to X-Class Solar Flares at the Great Wall Station in Antarctica. *Space Weather* **2023**, *21*, e2022SW003249. [CrossRef]
13. Yedemsky, D.Y.; Ryabov, B.S.; Shchokotov, A.Y.; Yarotsky, V.S. Experimental investigation of the tweek field structure. *Adv. Space Res.* **1992**, *12*, 251–254. [CrossRef]
14. Hayakawa, M.; Ohta, K.; Baba, K. Wave characteristics of tweek atmospherics deduced from the direction-finding measurement and theoretical interpretation. *J. Geophys. Res. Atmos.* **1994**, *99*, 10733–10743. [CrossRef]
15. Ammar, A.; Ghalila, H. Estimation of nighttime ionospheric D-region parameters using tweek atmospherics observed for the first time in the North African region. *Adv. Space Res.* **2020**, *66*, 2528–2536. [CrossRef]
16. Shvets, A.V.; Hayakawa, M. Polarisation effects for tweek propagation. *J. Atmos. Sol.-Terr. Phys.* **1998**, *60*, 461–469. [CrossRef]
17. Helliwell, R.A. *Whistlers and Related Ionospheric Phenomena*; Courier Corporation: Chelmsford, MA, USA, 1965. [CrossRef]
18. Streltsov, A.V.; Bengtson, M.T. Observations and modeling of whistler mode waves in the magnetospheric density ducts. *J. Geophys. Res. Space Phys.* **2020**, *125*, e2020JA028398. [CrossRef]
19. Williams, D.D.; Streltsov, A.V. Whistler-mode waves in the magnetospheric ducts: Statistical study. *J. Geophys. Res. Space Phys.* **2022**, *127*, e2022JA030462. [CrossRef]
20. Kumar, S.; Kishore, A.; Ramachandran, V. Higher harmonic tweek sferics observed at low latitude: Estimation of VLF reflection heights and tweek propagation distance. *Ann. Geophys.* **2008**, *26*, 1451–1459. [CrossRef]
21. Kumar, S. Tweek atmospherics: Diagnostics Tools to Probe D-Region Ionosphere. *AIP Conf. Proc.* **2010**, *1286*, 129–136. [CrossRef]
22. Reznikov, A.E.; Sukhorukov, A.I.; Edemskii, D.E.; Kopeikin, V.V.; Morozov, P.A.; Ryabov, B.S.; Shchekotov, A.Y.; Solov'Ev, V.V. Investigations of the lower ionosphere over Antarctica via ELF-VLF radiowaves. *Antarct. Sci.* **1993**, *5*, 107–113. [CrossRef]
23. Tan, L.M.; Thu, N.N.; Ha, T.Q.; Nguyen-Luong, Q. Seasonal variations of nighttime D-region ionosphere in 2013 solar maximum observed from a low-latitude station. *Earth Planets Space* **2015**, *67*, 163. [CrossRef]

24. Cohen, M.B.; Inan, U.S.; Paschal, E.W. Sensitive broadband ELF/VLF radio reception with the AWESOME instrument. *IEEE Trans. Geosci. Remote Sens.* **2009**, *48*, 3–17. [CrossRef]
25. Clilverd, M.A.; Rodger, C.J.; Thomson, N.R.; Brundell, J.B.; Ulich, T.; Lichtenberger, J.; Cobbett, N.; Collier, A.B.; Menk, F.W.; Seppälä, A.; et al. Remote sensing space weather events: Antarctic-Arctic radiation-belt (dynamic) deposition-VLF atmospheric research Konsortium network. *Space Weather* **2009**, *7*, S04001. [CrossRef]
26. Zhou, R.X.; Gu, X.D.; Yang, K.X.; Li, G.S.; Ni, B.B.; Yi, J.; Chen, L.; Zhao, F.T.; Zhao, Z.Y.; Wang, Q.; et al. Detailed investigation of low latitude tweek atmospherics observed by the WHU ELF/VLF receiver: I. Automatic detection and analysis method. *Earth Planet. Phys.* **2020**, *4*, 120–130. [CrossRef]
27. Golden, D.I.; Spasojevic, M.; Inan, U.S. Determination of solar cycle variations of midlatitude ELF/VLF chorus and hiss via automated signal detection. *J. Geophys. Res. Space Phys.* **2011**, *116*, A03225. [CrossRef]
28. Maslej-Krešňáková, V.; Kundrát, A.; Mackovjak, Š.; Butka, P.; Jaščur, S.; Kolmašová, I.; Santolík, O. Automatic detection of atmospherics and tweek atmospherics in radio spectrograms based on a deep learning approach. *Earth Space Sci.* **2021**, *8*, e2021EA002007. [CrossRef]
29. Xu, W.; Ma, W.; Wang, S.; Gu, X.; Ni, B.; Cheng, W.; Feng, J.; Wang, Q.; Hu, M. Automatic Detection of VLF Tweek Signals Based on the YOLO Model. *Remote Sens.* **2023**, *15*, 5019. [CrossRef]
30. Ohya, H.; Nishino, M.; Murayama, Y.; Igarashi, K. Equivalent electron densities at reflection heights of tweek atmospherics in the low-middle latitude D-region ionosphere. *Earth Planets Space* **2003**, *55*, 627–635. [CrossRef]
31. Shvets, A.; Serdiuk, T.; Krivonos, A.; Hayakawa, M. Automatic method for monitoring the lower ionosphere and lightning location by tweek-atmospherics. In Proceedings of the 2018 International Symposium on Electromagnetic Compatibility (EMC EUROPE), Amsterdam, The Netherlands, 27–30 August 2018; pp. 789–794. [CrossRef]
32. Ohya, H.; Shiokawa, K.; Miyoshi, Y. Daytime tweek atmospherics. *J. Geophys. Res. Space Phys.* **2015**, *120*, 654–665. [CrossRef]
33. Yi, J.; Gu, X.; Cheng, W.; Tang, X.; Chen, L.; Ni, B.; Zhou, R.; Zhao, Z.; Wang, Q.; Zhou, L. A detailed investigation of low latitude tweek atmospherics observed by the WHU ELF/VLF receiver: 2. Occurrence features and associated ionospheric parameters. *Earth Planet. Phys.* **2020**, *4*, 238–245. [CrossRef]
34. Maurya, A.K.; Singh, R.; Veenadhari, B.; Kumar, S.; Cohen, M.B.; Selvakumaran, R.; Pant, P.; Singh, A.K.; Siingh, D.; Inan, U.S. Morphological features of tweeks and nighttime D region ionosphere at tweek reflection height from the observations in the low-latitude Indian sector. *J. Geophys. Res. Space Phys.* **2012**, *117*, A05301. [CrossRef]
35. Maurya, A.K.; Veenadhari, B.; Singh, R.; Kumar, S.; Cohen, M.B.; Selvakumaran, R.; Gokani, S.; Pant, P.; Singh, A.K.; Inan, U.S. Nighttime D region electron density measurements from ELF-VLF tweek radio atmospherics recorded at low latitudes. *J. Geophys. Res. Space Phys.* **2012**, *117*, A11308. [CrossRef]
36. Tan, L.M.; Shiokawa, K.; Thu, N.N.; Ha, T.Q. Electron density variability of nighttime D region ionosphere in Vietnamese and Japanese sectors. *J. Geophys. Res. Space Phys.* **2017**, *122*, 6543–6551. [CrossRef]
37. Chen, Y.; Yang, G.; Ni, B.; Zhao, Z.; Gu, X.; Zhou, C.; Wang, F. Development of ground-based ELF/VLF receiver system in Wuhan and its first results. *Adv. Space Res.* **2016**, *57*, 1871–1880. [CrossRef]
38. Dowden, R.L.; Brundell, J.B.; Rodger, C.J. VLF lightning location by time of group arrival (TOGA) at multiple sites. *J. Atmos. Sol.-Terr. Phys.* **2002**, *64*, 817–830. [CrossRef]
39. Dowden, R.L.; Holzworth, R.H.; Rodger, C.J.; Lichtenberger, J.; Thomson, N.R.; Jacobson, A.R.; Lay, E.; Brundell, J.B.; Lyons, T.J.; O'Keefe, S.; et al. World-wide lightning location using VLF propagation in the Earth-ionosphere waveguide. *IEEE Antennas Propag. Mag.* **2008**, *50*, 40–60. [CrossRef]
40. Ibrahim, S.N.; Shariff KK, M.; Sulaiman, A.A.; Abdullah, M.; Hussin, M.F.; Al Junid, S.A.M. Locating tweeks atmospherics source locations using WWLLN data. In Proceedings of the 2013 IEEE International Conference on Space Science and Communication (IconSpace), Melaka, Malaysia, 1–3 July 2013; pp. 420–423. [CrossRef]
41. Appleton, E.V. Wireless studies of the ionosphere. *Inst. Electr. Eng.-Proc. Wirel. Sect. Inst.* **1932**, *7*, 257–265. [CrossRef]
42. Hartree, D.R. The propagation of electromagnetic waves in a stratified medium. In *Mathematical Proceedings of the Cambridge Philosophical Society*; Cambridge University Press: Cambridge, UK, 1929; Volume 25, pp. 97–120.

Disclaimer/Publisher's Note: The statements, opinions and data contained in all publications are solely those of the individual author(s) and contributor(s) and not of MDPI and/or the editor(s). MDPI and/or the editor(s) disclaim responsibility for any injury to people or property resulting from any ideas, methods, instructions or products referred to in the content.